

RESEARCH

Open Access



P4-ATPase subunit Cdc50 plays a role in yeast budding and cell wall integrity in *Candida glabrata*

Ke-Zhi Chen^{1,2†}, Lu-Ling Wang^{1,2†}, Jin-Yan Liu², Jun-Tao Zhao¹, Si-Jia Huang^{1,2} and Ming-Jie Xiang^{1,2*}

Abstract

Background As highly-conserved types of lipid flippases among fungi, P4-ATPases play a significant role in various cellular processes. Cdc50 acts as the regulatory subunit of flippases, forming heterodimers with Drs2 to translocate aminophospholipids. Cdc50 homologs have been reported to be implicated in protein trafficking, drug susceptibility, and virulence in *Saccharomyces cerevisiae*, *Candida albicans* and *Cryptococcus neoformans*. It is likely that Cdc50 has an extensive influence on fungal cellular processes. The present study aimed to determine the function of Cdc50 in *Candida glabrata* by constructing a $\Delta cdc50$ null mutant and its complemented strain.

Results In *Candida glabrata*, the loss of Cdc50 led to difficulty in yeast budding, probably caused by actin depolarization. The $\Delta cdc50$ mutant also showed hypersensitivity to azoles, caspofungin, and cell wall stressors. Further experiments indicated hyperactivation of the cell wall integrity pathway in the $\Delta cdc50$ mutant, which elevated the major cell wall contents. An increase in exposure of β -(1,3)-glucan and chitin on the cell surface was also observed through flow cytometry. Interestingly, we observed a decrease in the phagocytosis rate when the $\Delta cdc50$ mutant was co-incubated with THP-1 macrophages. The $\Delta cdc50$ mutant also exhibited weakened virulence in nematode survival tests.

Conclusion The results suggested that the lipid flippase subunit Cdc50 is implicated in yeast budding and cell wall integrity in *C. glabrata*, and thus have a broad influence on drug susceptibility and virulence. This work highlights the importance of lipid flippase, and offers potential targets for new drug research.

Keywords *Candida glabrata*, Lipid flippase, Cdc50, Drug susceptibility, Cell wall integrity, Virulence

Background

As the most common opportunistic fungi, *Candida* species are usually part of the human normal flora, yet retain the ability to cause both mucosal infection (e.g., thrush and vulvovaginal candidiasis) and invasive

candidiasis under certain conditions, such as improper usage of antifungal drugs or immunodeficiency virus infection [1–4]. In recent years, a worldwide increase in the prevalence of invasive candidiasis has been observed, which was mostly attributed to expanded immunocompromised populations [5–7]. Among all *Candida* species, *Candida glabrata* accounts for nearly 21% of the *Candida* bloodstream infections in Canada [8] and 24% of the systemic infections among USA transplant recipients [5], ranking only second to *Candida albicans*. Possessing the highest mortality rate among *Candida* species, hematogenous candidiasis caused by *C. glabrata* has remained a severe problem [9, 10]. Additionally, *C. glabrata* has been reported

[†]Ke-Zhi Chen and Lu-Ling Wang share first authorship.

*Correspondence:

Ming-Jie Xiang
mjxiang123456@126.com

¹ Department of Laboratory Medicine, Ruijin Hospital, Shanghai Jiao Tong University School of Medicine, Shanghai, China

² Department of Laboratory Medicine, Ruijin Hospital Luwan Branch, Shanghai Jiao Tong University School of Medicine, Shanghai, China



to quickly develop adaptation to moderate fungicidal azoles exposure [11–13]. However, there's no sufficient understanding concerning what makes *C. glabrata* the second most infectious *Candida*, considering that it lacks the yeast-hyphal switch or secreted aspartyl proteases like other *Candida* species [1, 2, 13]. More attention should be paid to *C. glabrata* to determine its pathogenic mechanism, with the aim of minimizing the damage it might cause.

P4-ATPases, a class of lipid flippases that drive the ATP-dependent translocation of aminophospholipids in eukaryotic cells, have attracted great attention in recent years [14–17]. P4-ATPases play a crucial role not only in physiological processes, but also in some clinically significant diseases. For example, ATP10A, a mutant form of human P4-ATPase, is implicated in type 2 diabetes, and ATP11A is implicated in tumor progression [14]. The broad influence of P4-ATPases is at least partly caused by their function in maintaining the asymmetric lipid distributions between eukaryotic membrane bilayers [18, 19]. Notably, the compositions of each leaflet are not symmetrically distributed: Phosphatidylcholine (PC) and sphingolipids are mostly located in the exoplasmic or luminal leaflet, while amino phospholipids (phosphoserine (PS) and phosphatidylethanolamine (PE)) occupy the cytoplasmic leaflet [18, 20, 21]. Such lipid gradients help in membrane budding and fission, thereby mediating various cellular processes, including secretory protein trafficking, cargo sorting, and signal transduction [21, 22].

Fungal P4-ATPases have been characterized in several previous studies. Consisting of α catalytic and β regulatory subunits, P4-ATPases are highly conserved among *Saccharomyces cerevisiae* and *Candida* species [21, 23]. To date, three homologs have been found in baker's yeast and *Candida* species: the Drs2-Cdc50 complex, the Dnf1/Dnf2-Lem3 complex, and Neo1 [24, 25]. Saito et al. [26, 27] first characterized the fungal Drs2-Cdc50 complex in *S. cerevisiae*, demonstrating that Drs2 and Cdc50 depended on each other to transport from the endoplasmic reticulum (ER) to the trans-Golgi network (TGN) membrane. The yeast $\Delta cdc50$ mutant showed defects in protein transport, actin organization, and vacuole structure in cold temperatures [27]. A screening test in 2016 [28] also found the loss of Cdc50 led to increased sensitivity to caspofungin in *Cryptococcus neoformans*. Furthermore, Cdc50 was reported to mediate azole susceptibility, cell wall and membrane integrity, and the response to pH and hyperosmotic stresses in *Cryptococcus neoformans* [28–30]. In the dimorphic fungi *Candida albicans*, besides having a hypersensitive phenotype to terbinafine, caspofungin, and azoles, the $\Delta cdc50$ mutant also possessed defective hyphal growth and virulence toward mice [23]. Given its strong conservation among

yeast-like fungi, the Cdc50 homolog presumably plays a similar role in *C. glabrata*.

In the present study, to determine the function of Cdc50, we constructed a $\Delta cdc50$ null mutant of *Candida glabrata* standard strain ATCC2001 via homologous recombination and a $\Delta cdc50 + CDC50$ complemented strain based on the null strain. The results implied that Cdc50 is required for yeast budding and cell wall integrity in *C. glabrata*, and thus have a broad influence on drug resistance and virulence. Furthermore, the cell wall integrity (CWI) pathway and downstream effector genes associated with cell wall biogenesis and remodeling were found to be constitutively upregulated in the $\Delta cdc50$ mutant.

Results

Loss of Cdc50 causes a moderate defect in cell growth and yeast budding in *C. glabrata*

Given that P4-ATPase subunit Cdc50 homologs in other common pathogenic fungi have a significant influence on cellular processes, a $\Delta cdc50$ null mutant and its complemented strain were constructed to study how it functions in *Candida glabrata*. First, the wild-type (WT), $\Delta cdc50$, and complemented strain $\Delta cdc50 + CDC50$ were incubated for 24 h, and their optical density (OD) at 600 nm was recorded to construct a growth curve (Fig. 1A). As the growth curve indicated, the $\Delta cdc50$ mutant showed defective cell growth, especially in exponential phase, during which other strains grew rapidly. However, after 24 h of incubation, the WT and $\Delta cdc50$ mutant ended up with similar optical densities, despite the OD of the WT being almost as twice that of $\Delta cdc50$ at 6 h. This implies that proper functioning of Cdc50 is required for rapid cell growth in *C. glabrata*.

Next, to demonstrate what causes the defective growth in the $\Delta cdc50$ mutant, we examined the cell cycle distributions of the WT and $\Delta cdc50$ mutant by microscopic observance, as shown in Table 1 and Fig. 1B. In the $\Delta cdc50$ mutant, the proportion of small-budded yeast increased from nearly 16% to 29% ($P < 0.05$), while large-budded yeast showed a slight decrease from 38 to 31%. The accumulation of small buds in cell cycle suggests that some of the $\Delta cdc50$ mutant cells have a difficulty in bud growth, which might be responsible for the observed cell growth defect.

As an essential cellular process for reproduction, yeast budding relies on the normal function of various accessory proteins, among which actin polarization plays a great part [31, 32]. During mitosis, actin undergoes rapid assembly and polarization to provide forces for morphogenesis. Disorganization of the actin cytoskeleton might easily disrupt bud growth and lead to cell cycle arrest. Actually, the budding block has been characterized in the

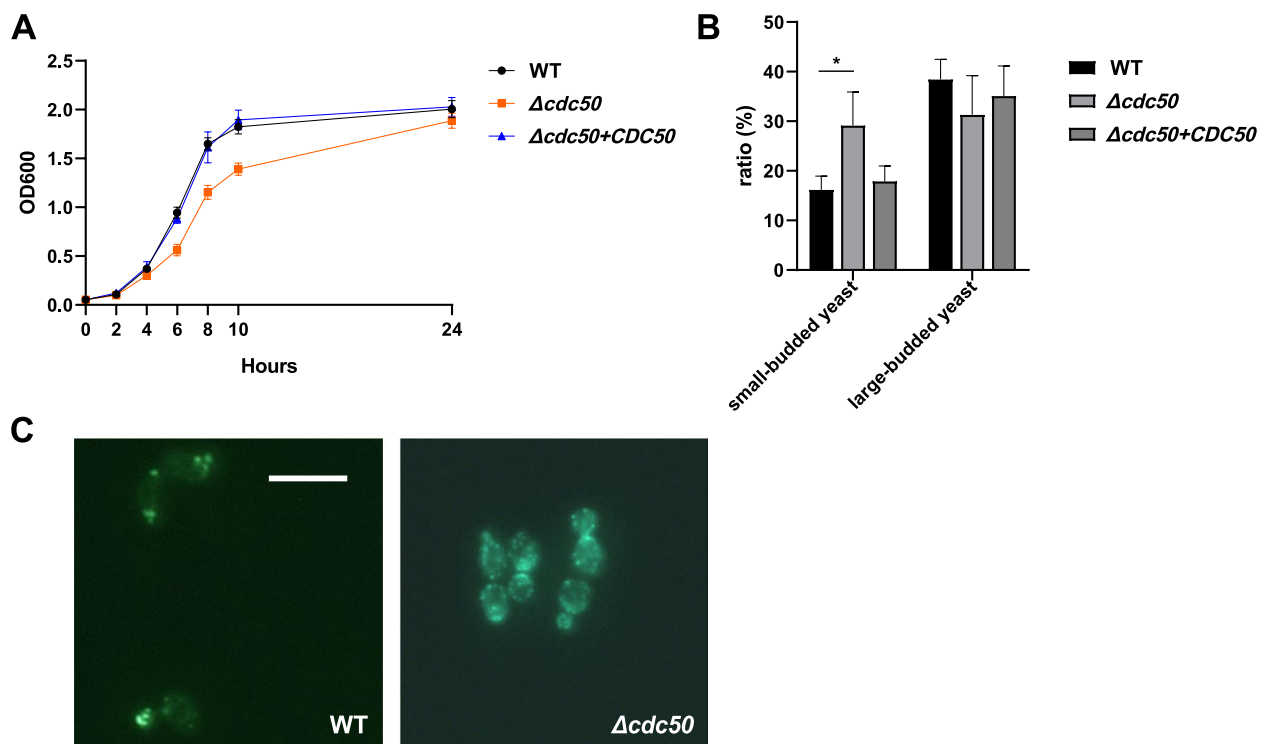





Fig. 1 The $\Delta cdc50$ mutant showed defects in cell growth, yeast budding, and actin polarization. **A** Wild-type (WT), $\Delta cdc50$, and $\Delta cdc50+CDC50$ strains were adjusted to the same cell density and incubated in fresh YPD medium at 30 °C for 24 h. Their OD at 600 nm was recorded to construct the cell growth curve. In the exponential phase, the $\Delta cdc50$ mutant exhibited significantly slower growth compared with the other two strains. **B** The cell cycle distribution of different strains as determined using microscopy. Mid-log phase yeast was collected and stained to be classified as having no, small, or large buds. More than 300 cells were counted in each group. The $\Delta cdc50$ mutant showed increased numbers of small buds and decreased numbers of large buds compared with those of the wild-type. Data represent the mean \pm SD of three independent experiments. **C** Typical views of wild-type and $\Delta cdc50$ actin fluorescent imaging during yeast budding. After staining with FITC-phalloidin, the WT and $\Delta cdc50$ yeast cells were observed using fluorescence microscopy. Most WT budding yeasts exhibited normal actin patch polarization (enriched in buds and bud necks), while a large amount of $\Delta cdc50$ budding yeasts showed actin mislocalization: The actin patches were depolarized and scattered. Bar, 10 μ m. *, $P < 0.05$. Data represent the mean \pm SD of three independent experiments

Table 1 Cell cycle distributions

	cell cycle distribution (% , mean \pm SD)		
	yeast with no bud	small-budded yeast	large-budded yeast
			
WT	45.71 \pm 6.24	16.17 \pm 2.76	38.45 \pm 4.04
$\Delta cdc50$	39.51 \pm 1.79	29.16 \pm 6.74	31.33 \pm 7.84
$\Delta cdc50+CDC50$	47.02 \pm 5.37	17.88 \pm 3.08	35.10 \pm 6.06

S. cerevisiae $\Delta cdc50$ mutant by Saito et al. [27], in which they attributed the yeast growth defect to actin patch depolarization and actin cable disappearance caused by mislocalization of proteins associated with actin organization, e.g., Bni1. Thus, to determine whether the actin

depolarization also occurred in the *C. glabrata* $\Delta cdc50$ mutant, actin staining using fluorescein isothiocyanate (FITC)-phalloidin was performed (Fig. 1C). Fluorescent imaging showed that most of the WT budding yeast exhibited normal actin patch polarization (enriched in

buds and bud necks), while a large amount of $\Delta cdc50$ budding yeast showed actin mislocalization, in which the actin patches were depolarized and scattered. These morphological observations suggested that the $\Delta cdc50$ mutant exhibited a growth defect and budding block, which might be at least partly caused by actin depolarization. For further validation, subcellular localization and null strain construction of the essential factors of cell polarity, such as Cdc42, may be needed.

The $\Delta cdc50$ mutant exhibits hypersensitivity to azoles and caspofungin

Azoles, polyenes and echinocandins are the most commonly used antifungal drugs. Considering that losing Cdc50 in other common yeasts has been reported to cause hypersensitivity to multiple drugs, both spot assays and reference methods of broth dilution were used to assess whether *C. glabrata* is required for surviving from azoles, amphotericin B, and caspofungin. As presented in Fig. 2A, the $\Delta cdc50$ mutant was hypersensitive to itraconazole and caspofungin, but displayed only slightly changed sensitivity to fluconazole, compared with that in the WT strain, and re-integrating *Cdc50* restored drug resistance.

Furthermore, we performed broth microdilution tests in Roswell Park Memorial Institute (RPMI)1640 liquid medium, the recommended method of the Clinical and Laboratory Standards Institute (CLSI), to quantify the drug susceptibility of different strains (Table 2). We found that the 50% minimum inhibitory concentration (MIC50) of fluconazole, itraconazole, voriconazole and caspofungin in the WT was respectively as four, four,

Table 2 MIC50 of different strains in RPMI1640 broth

Drug	MIC50 of strains at 48 h in RPMI1640 broth ($\mu\text{g/ml}$)		
	WT	$\Delta cdc50$	$\Delta cdc50 + CDC50$
fluconazole	1	0.25	1
itraconazole	0.125	0.031	0.125
voriconazole	0.25	0.125	0.25
caspofungin	0.125	0.016	0.125
amphotericin B	0.5	0.5	0.5

two and eight times that in the $\Delta cdc50$ mutant, which agreed with the results of the spot assays. This evidence indicated that the cellular defects of the $\Delta cdc50$ mutant might affect the establishment of drug tolerance. Interestingly, for amphotericin B, there was no significant difference between the susceptibility of the WT and $\Delta cdc50$ strains, whether on plates (data not shown) or in RPMI1640 broth (Table 2).

In terms of antifungal mechanisms, azoles target and suppress the ergosterol biogenesis pathway, an important process for the fungal plasma membrane, to cause membrane structure damage [11], while echinocandins specifically inhibit fungal β -(1,3)-glucan synthases to induce deficient cell walls lacking β -(1,3)-glucan, which fails to shelter cells from multiple outside stresses [34]. Increased sensitivity to azoles and caspofungin observed in the $\Delta cdc50$ mutant suggested some structural defects in cell membrane and cell wall, respectively.

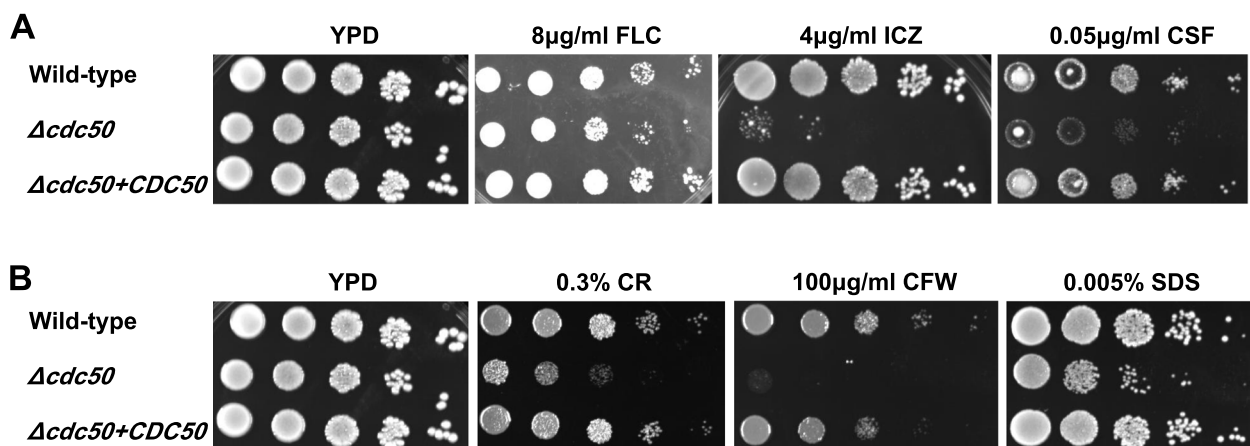


Fig. 2 The $\Delta cdc50$ mutant showed hypersensitivity to antifungal drugs and cell wall stressors. Mid-log phase yeast was adjusted to 0.1 OD at 600 nm and diluted tenfold serially to be spotted on YPD plates containing different drugs. **A** The $\Delta cdc50$ mutant exhibited weakened resistance to the clinically used antifungal drugs fluconazole, itraconazole and caspofungin. FLC, fluconazole; ICZ, itraconazole; CSF, caspofungin. **B** The $\Delta cdc50$ mutant was more sensitive to cell wall stressors CR, CFW and SDS, suggesting cell wall remodeling. CR, Congo Red; CFW, Calcofluor White; SDS, sodium dodecyl sulfate

Cdc50 disruption led to cell wall remodeling in *C. glabrata*

Since the $\Delta cdc50$ mutant possessed hypersensitivity to azoles and caspofungin compared with the WT strain, YPD plates containing 0.005% sodium dodecyl sulfate (SDS), 0.3% Congo Red and 100 $\mu\text{g}/\text{ml}$ Calcofluor White (CFW), respectively, were used for stress assays. Among these stressors, SDS works as a surfactant to dissolve the yeast cell membrane, which shows enhanced fungistatic activity with the existence of cell membrane or wall damage. Congo Red and CFW are chitin-binding agents often used to estimate cell wall integrity [35]. As shown in Fig. 2B, after growing for 48 h, the $\Delta cdc50$ mutant exhibited severe hypersensitivity to Congo Red and CFW compared with the WT and complemented strain, implying an altered cell wall in the $\Delta cdc50$ mutant. Besides, $\Delta cdc50$ yeast seemed to be weaker in response to SDS exposure, probably due to increased permeability of the cell wall.

As a highly-conserved structure in fungi, the cell wall plays a vital role, acting as a structural support and primary shield from various external stresses, such as mechanical, osmotic, oxidative and pH stresses [36]. It is composed of the inner β -(1,3)-glucan and chitin layer, which are the two main pathogen-associated molecular patterns (PAMPs) for host innate immune cell recognition, as well as the outer mannan skeleton and highly mannosylated protein branches that mask the inner layer, avoid recognition, and minimize host immune responses [2, 35, 37]. Any shortage in these compositions or change in structure may result in weakened stress resistance.

Loss of Cdc50 leads to increased cell wall components

To determine the reason for the defective cell wall in the $\Delta cdc50$ mutant, different fluorescent dyes combined with flow cytometry and spectrofluorometry were used to assess the cell wall compositions. FITC conjugated lectin from Concanavalin A (ConA), CFW and Aniline Blue were used for total mannan, chitin and β -(1,3)-glucan measurements, respectively. The data acquired was analyzed and the mean fluorescence intensities are presented in Fig. 3A. Interestingly, according to the results, all the major compositions of the $\Delta cdc50$ mutant were higher than those in the WT: The mannan content increased by 14.5% ($P < 0.05$), the chitin content increased by 39% ($P < 0.001$), and the β -(1,3)-glucan content increased by 44.3% ($P < 0.05$), indicating that losing Cdc50 might lead to a thicker cell wall in *C. glabrata*. Additionally, the increased cell wall chitin contents might be responsible for the CFW-sensitive phenotype of $\Delta cdc50$, as in the majority of cases, increased chitin was thought to be connected with hypersensitivity to CFW [38].

An increase in β -(1,3)-glucan and chitin exposure was detected on the $\Delta cdc50$ mutant cell surface

We have found that the total mannan, chitin and β -(1,3)-glucan contents in the $\Delta cdc50$ mutant were higher than those in the WT and complemented strain. However, since the inner cell wall layer is mostly masked behind the outer mannan layer, it is the exposure of glucan and chitin, not the total content that has the most influence on the host-*Candida* interaction [2, 37], which highlights the importance of exposure detection. FITC-conjugated wheat germ agglutinin (WGA), which binds N-acetylglucosamine specifically, was used to estimate the chitin exposure, while an anti- β -(1,3)-glucan monoclonal antibody was used to measure exposed β -(1,3)-glucan, as the dye and antibody molecules are too large to pass through the mannan skeleton and are only capable of binding to the exposed part of inner layer [39, 40]. The data acquired via flow cytometry showed that the exposure of β -(1,3)-glucan in the $\Delta cdc50$ mutant was increased by 25.5% ($P < 0.01$), and the exposure of chitin increased by 18.7% ($P < 0.001$) (Fig. 3B), which demonstrated that disrupting Cdc50 promoted unmasking of β -(1,3)-glucan and chitin on the cell surface.

The $\Delta cdc50$ mutant shows less uptake and enhanced pro-inflammatory cytokine secretion by macrophages

Increased β -(1,3)-glucan and chitin exposure on the cell surface is considered as a signal for innate immune cell recognition and phagocytosis, especially by macrophages. The unmasking of β -(1,3)-glucan and chitin in the $\Delta cdc50$ mutant suggested that Cdc50 might affect the interaction with host immune cells through cell wall alternations. Therefore, phagocytosis assays for THP-1 macrophages co-incubated with *C. glabrata* were performed, using both yeast counting and pro-inflammatory cytokine measurements to determine the yeast's ability to escape from phagocytosis and their survival and proliferation inside macrophages. First, plate colony forming units (CFU) counting after a 2-h co-incubation was performed. Surprisingly, the $\Delta cdc50$ mutant was subjected to much less phagocytosis (35%) than the WT (Fig. 4A) ($P < 0.05$). Moreover, after washing away the extracellular yeast, another plate was cultured for a further 4 h to detect the yeast proliferation capacity. The number of $\Delta cdc50$ mutant cells was only 60% compared with the WT cells ($P < 0.01$; Fig. 4A).

To further validate the decreased phagocytosis rate of the $\Delta cdc50$ mutant and eliminate the effect of Triton usage, we conducted the microscopic yeast counting. Macrophages after co-incubating with yeast for 2 h were brushed from the plate and Gram stained to count the intracellular yeast cells. As shown in Fig. 4B, the intracellular WT and complemented cells inside

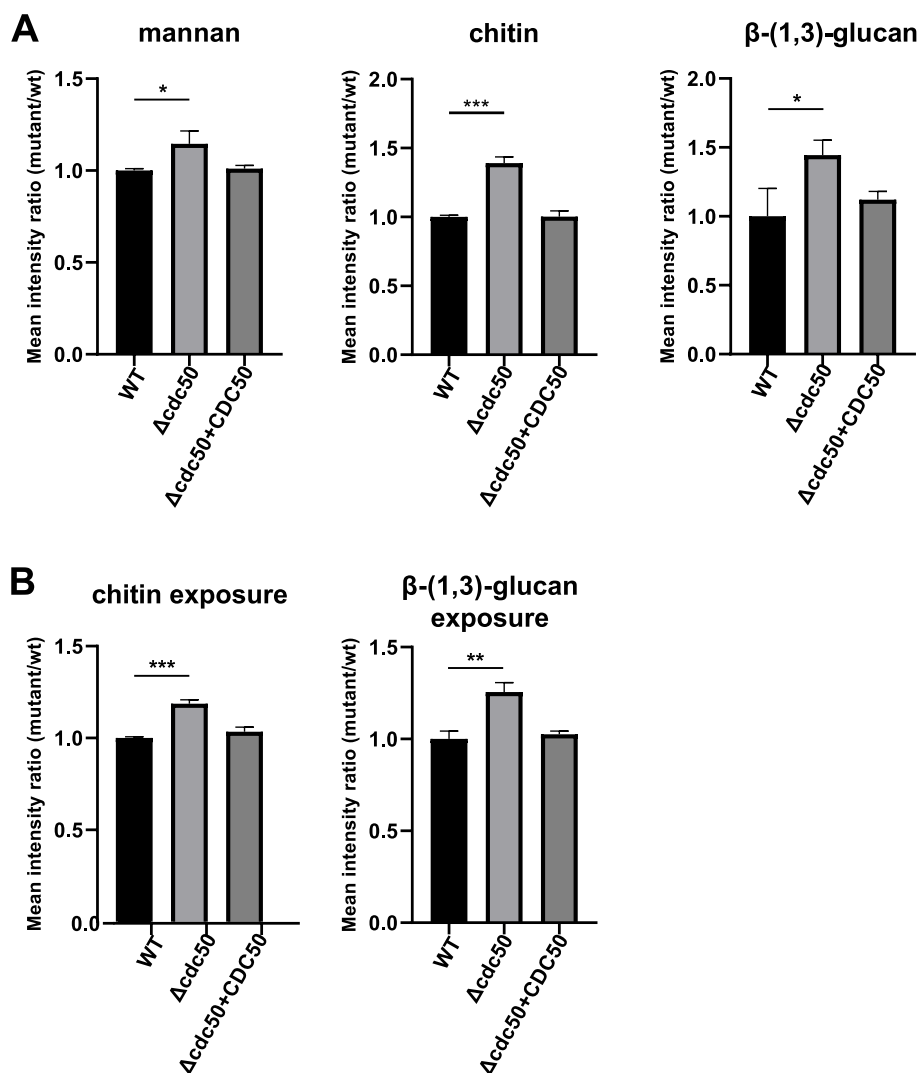


Fig. 3 Increased cell wall mannan, chitin and β -1,3-glucan contents, along with exposed chitin and β -1,3-glucan were found in $\Delta cdc50$. **A** Yeast cells in mid-log phase were collected and incubated in FITC-ConA, CFW and Aniline Blue to assess the total cell wall mannan, chitin, and β -1,3-glucan contents, respectively, then analyzed using flow cytometry and spectrofluorometry. In the $\Delta cdc50$ mutant, the cell wall mannan content increased by 14.5%, total chitin contents increased significantly by 39%, and total β -1,3-glucan contents increased by 44.3%. **B** Exposure of chitin and β -1,3-glucan were tested using FITC-WGA and anti- β -1,3-glucan antibodies. The exposure of inner chitin has increased by 14.9%, while the β -1,3-glucan exposure has increased by 25.5% in the $\Delta cdc50$ mutant. Data represent the mean \pm SD of three independent experiments. *, $P < 0.05$; **, $P < 0.01$; ***, $P < 0.001$

the macrophages were a little more than $\Delta cdc50$ cells ($P < 0.05$), and the typical views of WT and $\Delta cdc50$ were presented in Fig. 4C. As *Candida glabrata* is known for its survival and proliferation in macrophages to avoid other immune cells, especially neutrophil-mediated killing, the decrease in uptake by THP-1 cells may result in less surviving *C. glabrata* in the host [41].

In addition to direct phagocytosis, macrophages also secrete pro-inflammatory cytokines to recruit more immune cells in the immune response against *Candida* species. However, *C. glabrata*, among all the *Candida*

species, is known for minimizing cytokine secretion and suppressing inflammatory responses for immune escape [42, 43]. Therefore, we tested the levels of tumor necrosis factor alpha (TNF- α) and interleukin 1 beta (IL-1 β) cytokines in the THP-1 cell supernatant using a chemiluminescence method after co-incubating THP-1 and *C. glabrata* for 4 h. The cytokines secreted by THP-1 without exposure to *C. glabrata* were measured as a negative control. We observed an increase in TNF- α and IL-1 β secretion by 67.69% ($P < 0.01$) and by 29.62% ($P < 0.01$), respectively, in $\Delta cdc50$ mutant (Fig. 4D). Apparently,

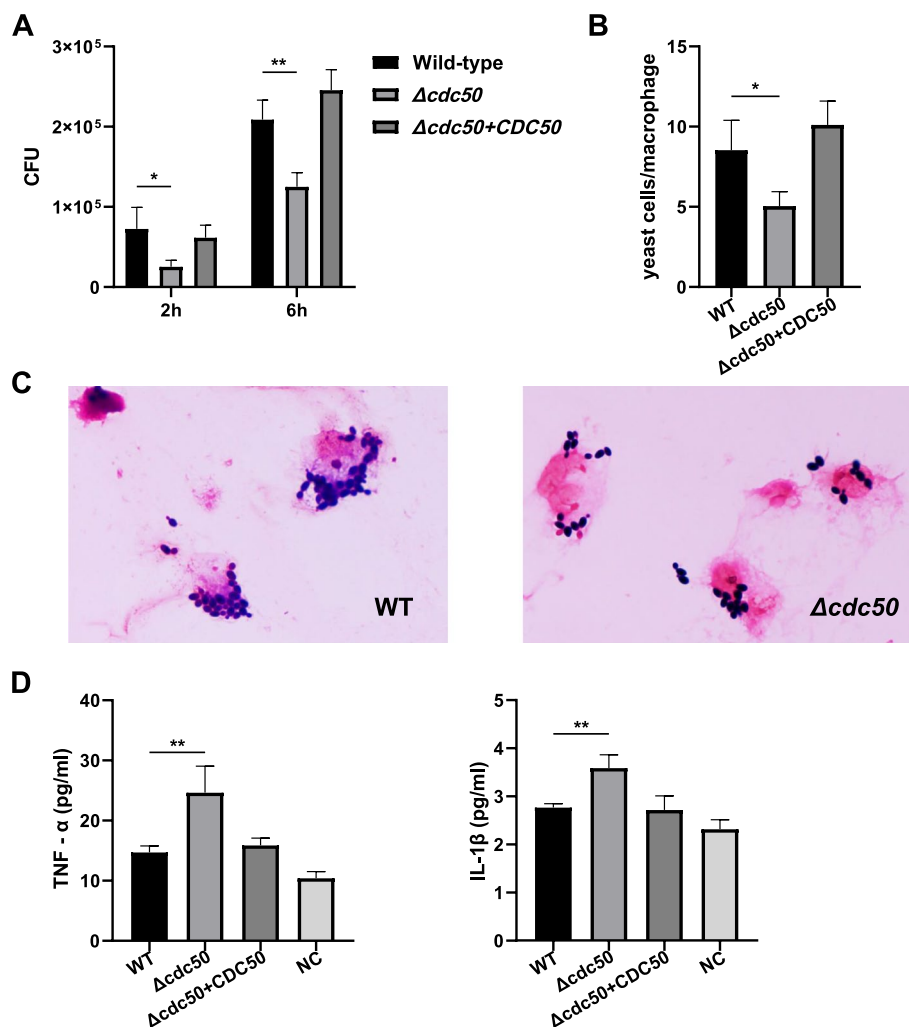


Fig. 4 Loss of Cdc50 led to decreased phagocytosis rate in macrophages and increased pro-inflammatory cytokine secretion. **A** Aliquots of THP-1 cells were co-incubated with wild-type (WT), $\Delta cdc50$, and $\Delta cdc50 + CDC50$ yeast for 2 h, then washed and lysed to release intracellular yeast for CFU counting. Other THP-1 cells were cultured for another 4 h after the 2-h co-incubation and washing, and lysed for CFU counting. After being exposed to macrophages for 2 h, the $\Delta cdc50$ mutant exhibited a much lower phagocytosis rate compared with the WT and $\Delta cdc50 + CDC50$ strains. Accordingly, the number of surviving intracellular $\Delta cdc50$ yeast were reduced by almost 50% compared with that of the surviving WT yeasts after 6 h. **B** After a 2-h co-incubation with yeast cells, THP-1 cells were brushed and Gram stained to count the intracellular yeast. The $\Delta cdc50$ cells were about 58.6% of WT cells, exhibiting less uptake by macrophages. **C** Typical field views of THP-1 after co-incubation with WT and $\Delta cdc50$ cells, respectively. **D** Different *C. glabrata* strains were co-incubated with THP-1 cells for 4 h, and the culture supernatants were collected and centrifugated to measure the secreted TNF- α and IL-1 β levels. THP-1 cells without exposure to yeast were used for baseline secretion level estimation as a negative control. Exposure to WT and $\Delta cdc50 + CDC50$ hardly triggered enhanced secretion of pro-inflammatory cytokines in macrophages, whereas the loss of Cdc50 activity in *C. glabrata* caused increased secretion of TNF- α and IL-1 β . Data represent the mean \pm SD of three independent experiments. NC Negative control. *, $P < 0.05$; **, $P < 0.01$

disruption of Cdc50 weakened the ability of *C. glabrata* to suppress THP-1 macrophages from secreting pro-inflammatory cytokines.

According to the results of CFU counting and cytokine measurements, we concluded that the $\Delta cdc50$ mutant showed attenuated immune escape, with decreased macrophage uptake and increased secretion of pro-inflammatory cytokines.

The $\Delta cdc50$ mutant shows weakened virulence toward *Caenorhabditis elegans*

We observed that Cdc50 is associated with cell wall integrity, which is of vital importance of fungal virulence; therefore, we carried out *C. elegans* survival assays to estimate the overall virulence of the $\Delta cdc50$ mutant in vivo. As a classical model organism that feeds on microorganisms, *C. elegans* is often used to evaluate

the virulence of fungal and bacterial pathogens [44]. Over 300 *C. elegans* were transferred to plates containing medium supporting *C. glabrata* growth, which were incubated for at least 25 days, during which the death count of each group was recorded daily to construct the survival curve shown in Fig. 5, and *Escherichia coli* OP50 strain was used as a quality control. In general, the lifespan of *C. elegans* feeding on $\Delta cdc50$ mutant was significantly longer compared with that for nematodes feeding on WT and $\Delta cdc50 + CDC50$ yeast ($P < 0.001$). Although *C. elegans* in different groups shared similar medium lifespans, thereafter nematodes exposed to the $\Delta cdc50$ yeast cells exhibited a much longer maximal lifespan. Disrupting Cdc50 allowed a larger number of nematodes to endure for a longer time, which might have something to do with the defective proliferation capacity that grows more and more visible over time, due to budding block and cell wall defect described before.

Overall, we conclude that losing Cdc50 led to weakened virulence of *C. glabrata* toward *C. elegans*.

The cell wall integrity (CWI) pathway is constitutively activated in the $\Delta cdc50$ mutant

Candida species have evolved several highly-conserved mechanisms in response to various external stresses, one of which is the CWI pathway. The whole CWI pathway consists of cell surface sensors, GTP/GDP exchange factors (GEFs), Rho family GTPases, protein kinases C (PKCs), the mitogen-activated protein kinase (MAPK) cascade, downstream transcription factors, and effectors [37]. To investigate the mechanism of cell wall remodeling in the $\Delta cdc50$ mutant, both quantitative real-time

reverse transcription PCR (qRT-PCR) and transcriptome sequencing (RNA-sequencing (RNA-seq)) were used to estimate the mRNA expression levels of MAPKs, downstream transcription factors and effectors associated with cell wall biogenesis.

Through qRT-PCR, we found that *Slt2*, encoding the already characterized MAPK in *C. glabrata* [45, 46], is constitutively upregulated in the $\Delta cdc50$ mutant, with an almost six-fold increase in transcription (Fig. 6A) ($P < 0.05$). The increasing trend was also seen in its downstream transcription factor-encoding genes *Rlm1*, *Swi4* and *Swi6*, whose expression levels increased by 429%, 298%, and 269% respectively (all $P < 0.001$). The cell wall biogenesis genes were also transcriptionally hyperactivated, with β -(1,3)-glucan synthase-encoding *Fks1* increasing by about three-fold, *Fks2* by six-fold, and chitin synthase-encoding *Chs3* by eight-fold (all $P < 0.001$). Thus, it appeared that the CWI pathway is constantly hyperactivated in the $\Delta cdc50$ mutant.

In the RNA-seq data, the differential expression genes (DEGs) between the WT and the $\Delta cdc50$ mutant were analyzed using Gene Ontology (GO) to reveal the pathways implicated in Cdc50 disruption. Unsurprisingly, the top 12 identified pathways were mostly associated with fungal cell wall organization and biogenesis (Fig. 6B). More specifically, 31 genes annotated with top 10 pathways were selected and visually compared in a heatmap (Fig. 6C). According to the heatmap, among these DEGs, *Pir3*, *Toh1*, *Yps1* and *Dfg5*, which all encode glycosyl phosphatidyl inositol (GPI)-anchored proteins, are associated with cell wall integrity, and all of them were transcriptionally activated in

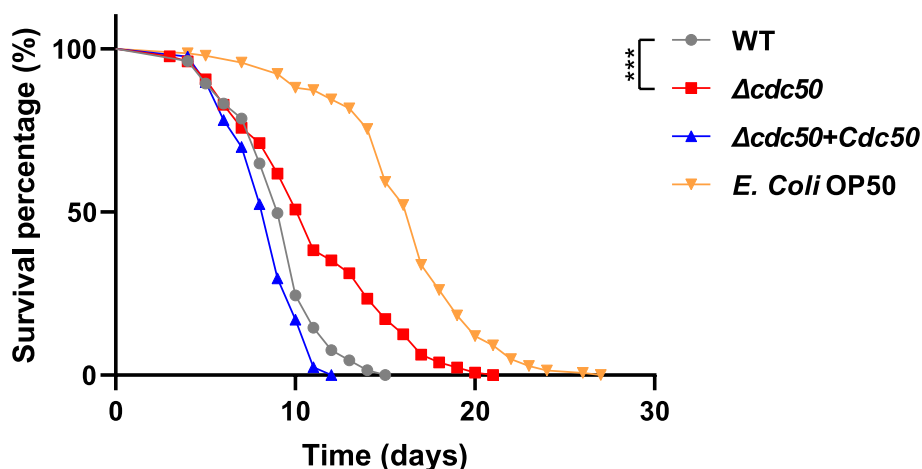


Fig. 5 The $\Delta cdc50$ mutant showed defective virulence in *Caenorhabditis elegans* compared with other strains. *C. elegans* were raised and fed on different strains of *C. glabrata*, and the number of deaths in each group was counted daily to construct a survival curve and assess in vivo virulence. *E. coli* OP50 strain was used as a quality control. Nematodes in the $\Delta cdc50$ group exhibited a longer lifespan compared with the wild-type (WT) and $\Delta cdc50 + CDC50$ group, suggesting weakened virulence in the $\Delta cdc50$ mutant. ***, $P < 0.001$

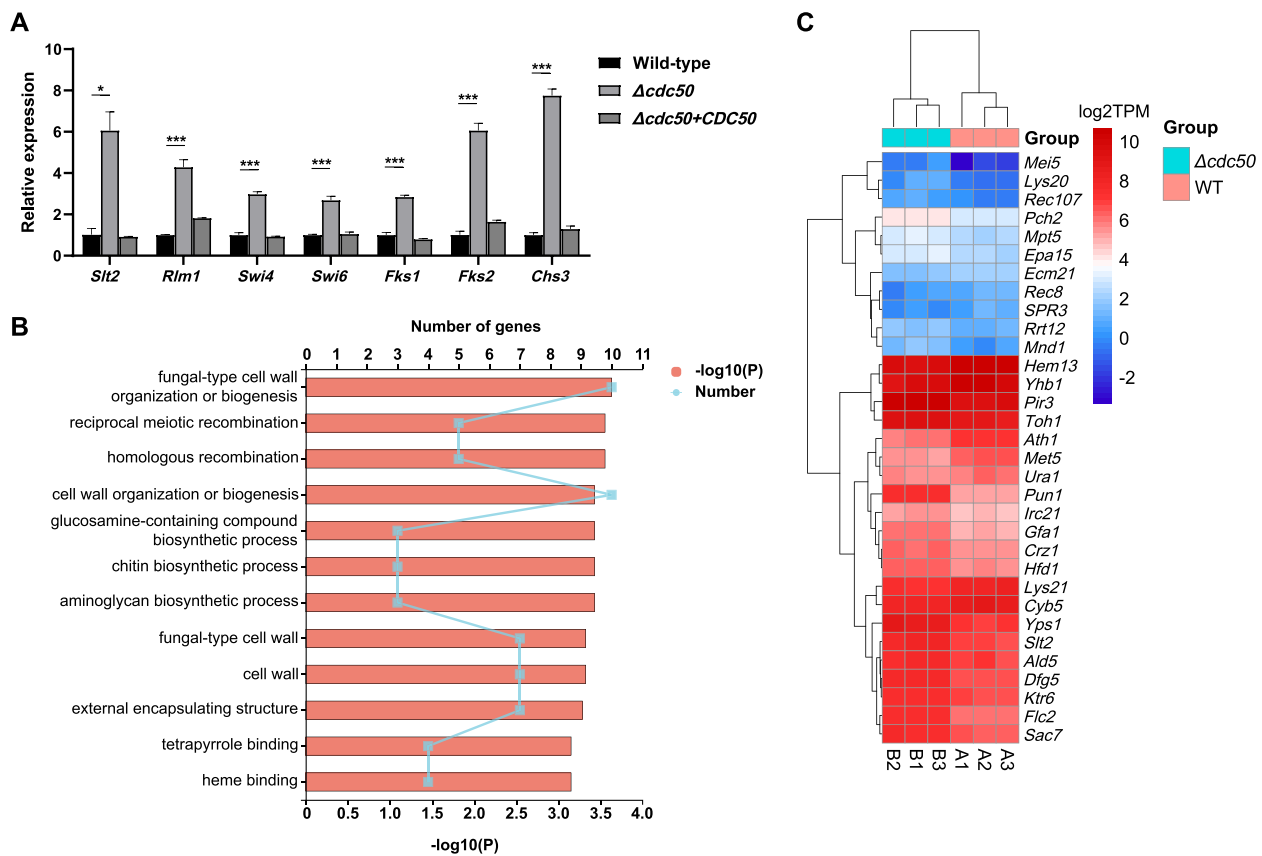


Fig. 6 Stress response pathways associated with cell wall biogenesis and remodeling were constitutively upregulated in the $\Delta cdc50$ mutant. **A** Mid-log phase yeast was collected, washed, and frozen to isolate total RNA, followed by qRT-PCR. The relative expression of genes in different strains were obtained by comparison with that in the wild-type (WT). In the $\Delta cdc50$ mutant, the genes that encode the constituents of the cell integrity pathway, including *Slt2*, *Rlm1*, *Swi4*, *Swi6*, *Fks1*, *Fks2* and *Chs3*, all showed increased expression to varying degrees. **B** Mid-log phase WT and $\Delta cdc50$ yeast were collected for complex transcriptome sequencing, and the expression level of every gene was quantified using the TPM method. Differentially expressed genes were enriched via GO functional enrichment analysis to identify significantly different GO pathways between the WT and $\Delta cdc50$. The top 12 most significant pathways were mainly implicated in cell wall organization and biogenesis. **C** The TPM of genes enriched in the GO pathways in **B** were gathered and taken the logarithm to generate a heatmap for visualized comparison. TPM, transcripts per million reads; GO, Gene Ontology. *, $P < 0.05$; **, $P < 0.01$; ***, $P < 0.001$

the $\Delta cdc50$ mutant, suggesting cell wall-stressed conditions. Moreover, *Sac7*, whose homolog in *S. cerevisiae* encodes a Rho family GTPase activating protein, and *Slt2*, both showed upregulated expression, which demonstrated activation of the CWI pathway. Interestingly, *Crz1*, encoding the downstream transcription factor of the calcineurin pathway, and *Flc2*, encoding the putative calcium channel protein involved in stress responses, were also upregulated, which might be considered as a sign of global stress response induction in $\Delta cdc50$ mutant.

Altogether, the transcriptional evidence from qRT-PCR and RNA-seq correspond with the increase in cell wall components mentioned above, indicating that cell wall biogenesis and remodeling of the $\Delta cdc50$ mutant is constitutively hyperactivated, and stress response pathways are upregulated.

Discussion

Among all the common *Candida* species, *Candida glabrata* is rather distinctive. It possesses no secreted hydrolases or pseudohyphae structures for invasive growth, let alone the capacity for white-opaque switching [1, 13]. Yet it remains an evolutionarily successful opportunistic pathogen, contributing to 10–20% of invasive candidiasis in Europe [4], with a 50% mortality rate among bloodstream infection populations, suggesting we should pay more attention to the underlying virulence factors. Meanwhile, acquired drug resistance in *Candida* species during antifungal treatment has risen to be a severe problem worldwide in recent decades [11, 12]; narrow range of antifungal drug classes has made this situation worse. Thus, further investigations into virulence factors or potential new antifungal targets are warranted.

Cdc50, a regulatory subunit of the P4-ATPase lipid flippase, has been reported to be required for protein trafficking, virulence, and azole and echinocandin tolerance in *S. cerevisiae*, *C. albicans* and *C. neoformans* [22, 47]. In *S. cerevisiae*, Cdc50 has been characterized to bind the catalytic subunit Drs2, helping to translocate aminophospholipids between the membrane bilayers to maintain the dynamic lipid asymmetry [26]. The Drs2-Cdc50 complex is localized to the TGN and late endosome membrane, while the homolog P4-ATPase in *S. cerevisiae*, the Dnf1-Lem3 complex, is localized to the plasma membrane, implying a spatial and functional differentiation in lipid flippases [26]. In the present report, we determined that Cdc50 has an influence on yeast budding and drug susceptibility in *C. glabrata*, which corresponds with the results of studies in other fungi, suggesting that P4-ATPases act as evolutionarily conserved proteins in fungi.

As a subunit of lipid flippase, why is fungal Cdc50 so widely influential? Perhaps it acts through the lipid asymmetry that forms the foundation of various cellular processes. On the one hand, the asymmetric distributions of differently charged aminophospholipids provide electronic charge conditions for proteins to bind or dissociate from the leaflet via electrostatic interactions. On the other hand, lipid gradients allow the existence of membrane curvature, enable membrane budding and fusion, and consequently, promote protein transport, secretion and internalization [15]. In the absence of lipid flippases, the membrane system remains stationary, causing trouble for inter- and intracellular material communications.

In this study, we first characterized the alterations in actin organization in the *C. glabrata* $\Delta cdc50$ mutant, which were first recognized in *S. cerevisiae* in 2004 [26]. During the lifecycle of yeast, frequent actin reorganization plays an essential part in morphogenesis, providing support for cellular processes such as vesicle internalization and budding growth. Fast polarization and disassembly of actin cables and patches requires the precise regulation and activation of at least 100 highly conserved accessory proteins [31, 48, 49]. For instance, at bud emergence, Rho family GTPase Cdc42 acts as a key regulator to recruit various effectors, e.g., Bni1 and Gic2, to promote actin cable polarization and actin patch clustering. Therefore, we developed a hypothesis to explain the actin mislocalization that was observed in the $\Delta cdc50$ mutant: By losing lipid flippase activity, the disrupted lipid asymmetry hindered protein trafficking, leading to mislocalization and malfunction of certain accessory protein, thus disturbing actin organization. This was partly supported by the work of Das et al. [50], who reported that losing Lem3, a Cdc50 family protein, led to alterations in the

electronic charges of the plasma membrane, thus triggering failure to extract Cdc42 from the membrane.

Hypersensitivity to azoles has been reported in *C. albicans*, *C. neoformans*, and *C. glabrata* after disturbing the function of lipid flippases, exhibiting high conservation among yeasts. Although this susceptibility has received little further research attention, a report published in 2015 [47] offers an explanation. The authors reported that by flipping PS between the membrane bilayers, the Cdc50-Drs2 flippase system in *S. cerevisiae* appeared to play a crucial part not only in cargo protein sorting, but also in ergosterol enrichment in the plasma membrane. Besides, this defect was thought to be achieved by mislocating the oxysterol-binding protein homologue, Kes1/Osh4. Thus, in *C. glabrata*, lipid flippases might also be required to control ergosterol's subcellular distribution by regulating the localization of specific accessory proteins, and the loss of flippase activity might result in a defective membrane, making it vulnerable when exposed to azoles. In agreement with this hypothesis, in *S. cerevisiae*, the synthetic lethality of mutations in *Cdc50* and genes associated with the late steps of ergosterol biogenesis (*Erg2~6*) were discovered [51]. Besides, hypersensitivity to drugs affecting phospholipid metabolism (cinamycin and miltefosine) was observed in the *C. neoformans* $\Delta cdc50$ mutant, implying altered membrane phospholipids [29]. Further studies, including membrane composition analysis combined with accessory protein localization, are required to determine the mechanism underlying this defect.

Another significant phenotype we observed in the $\Delta cdc50$ mutant was cell wall remodeling, which has also been reported in *C. neoformans* [28]. We observed hypersensitivity to Congo Red and CFW, which is usually implicated in increased chitin contents in the cell wall. Further fluorescence staining showed increase in all the three major cell wall components. The increase in the chitin content is thought to correlate positively with tolerance to caspofungin, but the β -(1,3)-glucan content usually correlates negatively with caspofungin tolerance [38, 52]; therefore, the hypersensitivity to caspofungin in the $\Delta cdc50$ mutant seems to be the result of both changes. Moreover, a thicker outer cell wall mannan layer is usually connected with better masking of the inner glucan and chitin; but to our surprise, an increase was observed not only for cell wall mannan contents, but also for the inner chitin and β -(1,3)-glucan exposure on the cell surface. A possible explanation is that loss of Cdc50 causes rearrangements of the cell wall, which changes the mannan structure and results in unmasking of the inner cell wall layer.

For the yeast-macrophage interaction, while most common *Candida* species have evolved a well-masked inner

layer for strategic avoidance, *C. glabrata* has evolved a well-regulated remodeling system to survive and reproduce inside macrophages instead [2, 43]. Some researchers even believe that *C. glabrata* favors being taken up by, and proliferating in macrophages to avoid instant killing by neutrophils [41]. Correspondingly, the exposure of inner cell wall glucan and chitin in *C. glabrata* is reported to be naturally much higher than in other *Candida* species [36, 38]. Therefore, the decrease in the phagocytosis rate of the $\Delta cdc50$ mutant was not likely to favor host survival and can be considered as a weakened virulence factor. Nonetheless, it was still surprising that more glucan and chitin exposure on the $\Delta cdc50$ cell surface did not induce increased uptake by macrophages, but this apparent paradox is not unique. In a study published in 2020 [39], in which different clinical *Candida* isolates were treated with sub-MIC concentration caspofungin, strains with increased cell wall glucan and chitin exposure also experienced reduced phagocytosis rate, whose mechanism remains unclear.

The highly conserved CWI pathway was found to be constitutively activated in the $\Delta cdc50$ mutant, along with the calcineurin stress response pathway. Under normal conditions, the CWI pathway is suppressed to a basal expression level to cover the regular demands of cell wall biogenesis [37]. However, once cell wall damage occurs, the cell surface sensors recognize it and deliver the signal to GEFs, which subsequently activate GTPases, PKCs, and MAPKs by phosphorylation at specific sites. Eventually, the pathway leads to the upregulated expression of effectors associated with cell wall biogenesis, such as β -(1,3)-glucan synthases Fks1~2 and chitin synthases Chs1~5, to restore cell wall integrity. The calcineurin pathway is involved in various stress responses, working via upregulation of calcium channels to activate downstream effectors [53]. Given the budding block, thicker cell wall and weakened resistance to stressors and antifungal agents associated with loss of Cdc50, we considered this abnormal hyperactivation of response pathways as a consequence of response dysregulation caused by mislocalization and malfunction of certain key

regulators, rather than cell wall damage. This is similar to the situation in *C. neoformans* [30], in which the authors observed hyperactivation of the calcineurin pathway and an abnormal increase in the cellular calcium level in the $\Delta cdc50$ mutant, which was considered to be responsible for increased sensitivity to caspofungin. In agreement, this hypersensitivity was reversed by disrupting a mechanosensitive calcium channel, Crm1, via restoring the calcium hemostasis.

Herein, we investigated the general role played by Cdc50 in cellular processes. We determined that Cdc50 has an extensive influence on yeast budding, drug resistance, cell wall integrity and macrophage uptake of *C. glabrata*. To study the underlying mechanisms, further experiments, e.g., determining the localization of significant accessory proteins, are needed. The importance of, and high conservation among fungi lipid flippases also offers potential targets for new drug research. In fact, a newly designed antifungal drug targeting the P4-ATPase function, the “AW9-Ma peptide”, has been reported to restore *C. neoformans*' sensitivity to caspofungin [54]. Considering the lack of newly-developed clinical antifungal drugs, these studies are particularly meaningful.

Conclusion

In the present study, we investigated the function of lipid flippase subunit Cdc50 in *C. glabrata* by constructing a $\Delta cdc50$ null mutant. Loss of Cdc50 led to difficulty in yeast budding, hypersensitivity to azoles, caspofungin and cell wall stressors. Further experiments indicated hyperactivation of the cell wall integrity pathway in the $\Delta cdc50$ mutant, which resulted in elevated major contents in the cell wall. The $\Delta cdc50$ mutant also exhibited weakened virulence in nematode survival tests. This work highlights the importance of lipid flippase, and offers potential targets for new drug research.

Materials and methods

Strains and media

The *Candida glabrata* strains and plasmids used in this study are listed in Table 3. All strains were routinely

Table 3 Strains and plasmids used in this study

Strain and plasmids	Genotype or description	Source or reference
ATCC2001	<i>Candida glabrata</i> ATCC2001 (CBS138) strain	ATCC
pYC44	The empty backbone for yeasts, NAT	Addgene
$\Delta cdc50$	ATCC2001 ($\Delta cdc50::NAT$)	This study
$\Delta cdc50 + CDC50$	ATCC2001 ($\Delta cdc50::NAT$, pCN-HygR-Cdc50)	This study
pCN-PDC1-GFP	The integrating vector of <i>C. glabrata</i> , NAT, GFP	Addgene
pCN-HygR-Cdc50	pCN-PDC1-GFP ($\Delta nat::HygR$, $\Delta gfp::Cdc50$)	This study
ATCC22019	<i>Candida parapsilosis</i> ATCC22019 strain	ATCC

maintained at 30 °C in yeast-peptone-dextrose (YPD) medium (1% yeast extract, 2% peptone, and 2% glucose) or on solid YPD medium (liquid YPD medium with 1.5% agar). YPD plates containing 100 µg/ml nourseothricin and 1000 µg/ml hygromycin were used when excising the NAT and hygR selective markers, respectively. Antifungal drugs were obtained from MCE (Monmouth Junction, NJ, USA) and Sigma-Aldrich (St. Louis, MO, USA).

Construction of the *C. glabrata* Δ *cdc50* null mutant and complemented strains

To knockout the *Cdc50* gene in *C. glabrata*, a NAT cassette containing a nourseothricin resistance marker was used for homologous recombination, as described previously [55]. Briefly, the upstream and downstream regions of *Cdc50* were amplified using the DNA of strain ATCC2001 as the template and primers Cdc50-UP and Cdc50-DOWN, and the NAT marker was amplified using plasmid pYC44 and primers NAT-Cdc50 (the reverse complement sequences are marked in lower case in Table 4). After fusion PCR, a knockout cassette was transformed into the ATCC2001 strain, as described previously by Zhao et al. [55]. Δ *cdc50* transformants that could grow on plates containing 100 µg/ml nourseothricin were selected and their genotypes were confirmed using PCR with primers *y-incdc50* and *y-outcdc50*. Next, to generate a reintegration strain, plasmid pCN-HygR-Cdc50 with a hygromycin resistance marker and the full-length *Cdc50* gene was constructed from pCN-PDC1-GFP using an In-fusion cloning kit (Takara, Shiga, Japan). After the transformation of pCN-hygR-Cdc50, colonies able to grow on a YPD plate with 1000 µg/ml hygromycin were selected as complemented strains, with further confirmation using qRT-PCR.

Cell growth, cell cycle distribution and budding assays

Yeast growing overnight in YPD medium at 30 °C were resuspended in new YPD medium and adjusted to 0.05 OD at 600 nm. After the concentration adjustments, the yeast was incubated at 30 °C, and their OD values were recorded after 2, 4, 6, 8, 10, and 24 h to construct a cell growth curve. For cell cycle examinations, yeast grown overnight was washed and incubated in new YPD medium for 4 h. Yeast in mid-log phase was smeared, fixed, Gram stained, and observed using optical microscopy at a 100× magnification. At least 300 yeast cells in each group were counted and classified as yeast with no bud, small-budded yeast, and large-budded yeast, to determine the cell cycle distribution as shown in Table 1. The entire experiments were repeated three times.

Table 4 Primers used in this study

Primer name	Sequence (5' → 3')
Cdc50-UP-F	AGTGAAGAGCAGCAACTCCC
Cdc50-UP-R	cccggacagccgctaggaggTCTGGCTCAGCCTACAGAGT
Cdc50-DOWN-F	ccgtagccccgatagtcgccgagACACCTGATGCTGGTGGTAAT
Cdc50-DOWN-R	ATCGGAGGTCCAGCTCATCT
NAT-Cdc50-F	acctcctagcggctgtccgggGTTGTAAAACGACGGCCAGT
NAT-Cdc50-R	ctcgggactatcgggctacggAGGAAACAGCTATGACCATG
<i>y-incdc50</i> -F	CACGCCAATTAGGAGGTGGT
<i>y-incdc50</i> -R	GCTAGCAAGGCCAGATGGAA
<i>y-outcdc50</i> -F	AGTGAAGAGCAGCAACTCCC
<i>y-outcdc50</i> -R	ACCACCAGCATCAGGTGTTA
RT-ACT1-F	TTCCAGCCTTCTACGTTTCC
RT-ACT1-R	TCTACCAGCAAGGTCGATTC
RT-SLT2-F	GAGGCAAGCGAGGAGACTAC
RT-SLT2-R	CGCATCTGTTAGTGCTTGCC
RT-RLM1-F	GTCACCGTAAGCAGAAGGCT
RT-RLM1-R	TCTTGAAGCGTAAAGCGGGT
RT-SWI4-F	TACGTCATCTGGCATGGCTC
RT-SWI4-R	TCCAATGGCACCCAAGTACC
RT-SWI6-F	AACCCGTTTAGCCTCCACTG
RT-SWI6-R	TCACTTGCAAGCTCGTGCT
RT-FKS1-F	TTGTCGACGGTCTTACGTT
RT-FKS1-R	GTAGGCAGCTGGTGGTTGAT
RT-FKS2-F	CTGGTGTGGCAATGGGTTG
RT-FKS2-R	AGCTGGGTATGGGTCGTTTG
RT-CHS3-F	AATGCCTGAGAAGGCCAGAC
RT-CHS3-R	ATCCTTCTGTCAGCAGACC

Note: Lower case letters indicate the reverse complement sequences

Fluorescent staining of actin

Actin staining was performed using Actin-Tracker Green dye (KeyGEN, Nanjing, China), following the manufacturer's instructions. Briefly, mid-log phase yeast was collected and washed three times with phosphate-buffered saline (PBS). After being fixed in 4% paraformaldehyde solution for 10 min, the yeast was blocked in PBS buffer containing 1% bovine serum albumin (BSA) and then stained using Actin-Tracker Green solution for 20 min in the dark. Then, the yeast was washed three times with PBS and observed using fluorescent microscopy with an Axio Scope A1 microscope (Zeiss, Oberkochen, Germany), with typical field views of each group being photographed.

Antifungal susceptibility tests and assays for stress responses

For the spot assays, yeast grown overnight in YPD medium at 30 °C were resuspended and grown in new YPD medium for 4 h. Mid-log phase cells were adjusted

to 0.1 OD at 600 nm, serially diluted by tenfold, and 10 μ l of each dilution was spotted onto YPD plates containing different antifungal agents. Phenotypes were recorded and photographed after growing at 30 °C for 36 h. The reference method for broth dilution antifungal susceptibility testing was followed according to the CLSI M27-S3 guidelines. Briefly, drugs were double diluted 10 times and added to 96-well plates containing mid-log phase yeast resuspended in RPMI1640 medium, with the *Candida parapsilosis* reference strain ATCC22019 used for quality control. The 50% minimum inhibitory concentrations (MIC50) of each strain were read after a 48-h incubation at 37 °C. The experiments were repeated three times.

Chitin, mannan and β -1,3-glucan measurements

For cell wall component assessments, FITC conjugated lectin from ConA (Sigma Aldrich), CFW (Sigma-Aldrich) and Aniline Blue (Sigma-Aldrich) were used to estimate total cell wall mannan, chitin and β -1,3-glucan contents, respectively. To further investigate the exposure of inner layer materials on the cell surface, FITC-conjugated WGA (Sigma-Aldrich) and anti- β -1,3-glucan mouse monoclonal antibodies (anti-glucan Ab) (Biosupplies, Yagoona, Australia) combined with goat anti-mouse IgG second antibodies-FITC (Abcam, Cambridge, MA, USA) were used to estimate the exposed mannan and β -(1,3)-glucan contents, respectively. Briefly, mid-log phase yeast cells were collected and washed twice with PBS, and then incubated with different stains in the dark for 30 min. After washing twice with fluorescence-activated cell sorting (FACS buffer), the yeast was analyzed using a FACS-Canto II flow cytometer (BD Biosciences, San Jose, CA, USA). The β -1,3-glucan measurements were performed as described by Lee and Kim [56]: after washing with PBS buffer, the yeast cells were incubated in 1 M NaOH at 80 °C for 30 min. Then, 300 μ l of Aniline Blue mix (40: 21: 59 of 0.1% aniline blue, 1 N HCl, and 1 M glycine/NaOH (pH 9.5)) was added to the tubes, incubated at 50 °C for 30 min and at room temperature for another 30 min. The fluorescent density was analyzed using a BioTek Synergy Neo2 multimode microplate reader (Berten Instruments, Montpelier, VT, USA). For β -(1,3)-glucan exposure estimation, the procedure was carried out as described by Chen et al. [40]: besides the incubation and washing, a preliminary block was needed before staining to avoid potential non-specific binding. The raw data acquired were then analyzed using FlowJo software (v.10.8.1; FlowJo LLC, Ashland, OR, USA).

***Candida*-macrophage interaction assays**

The *Candida*-macrophage interaction assays were performed as described by Hu et al. [29]. Briefly, the

monocyte-like cell line THP-1 was grown in RPMI1640 medium containing 10% fetal bovine serum at 37 °C with 5% CO₂. The THP-1 cells were then adjusted to a concentration of 1×10^6 cells/ml and added to 24-well plates (0.5 ml per well) with fresh medium containing 100 ng/ml phorbol-12-myristate-13-acetate (Sigma-Aldrich) for differentiation and adherence induction. After 24 h of stimulation, the cells were washed and relaxed overnight before the phagocytosis assay. Mid-log phase yeast cells were collected as described above and adjusted to 0.5 OD at 600 nm. After being diluted tenfold with RPMI1640 medium, the yeast was added to 12-well plates and co-incubated with THP-1 cells for 2 h at 37 °C with 5% CO₂. For the phagocytosis colony counting, after a 2-h incubation, the cells were washed three times with PBS buffer to wash away extracellular yeast. While one plate was ready for digestion, another plate was prepared for a further 4-h incubation after washing to assess the survival of the intracellular yeast. To lyse the macrophages and release the yeast inside, 0.5% Triton X-100 solution was added to the 12-well plates. After a 5-min incubation, the lysate was centrifugated at $4000 \times g$ for 5 min, then resuspended in PBS and diluted 1000-fold. The diluent was spread on YPD plates, cultured at 30 °C for 48 h, and the colonies were counted to estimate the number of intracellular yeast cells. Meanwhile, after a 2-h incubation, the THP-1 cells were washed three times with PBS buffer, followed by being brushed using cytology brushes and Gram stained for microscopic yeast counting. At least 200 THP-1 cells in every group were observed to count the intracellular yeast cells. For cytokine measurements, after a 4-h co-incubation of THP-1 and yeast cells, the supernatants were collected, centrifugated at $10,000 \times g$ for 5 min, and then the cytokines were analyzed using chemiluminescent immunoassays with the Immulite1000 system (Siemens, Munich, Germany). THP-1 cells without exposure to *C. glabrata* were used to measure the baseline level of secreted cytokines. The phagocytosis assays were repeated three times.

Survival assays of *Caenorhabditis elegans*

To investigate the virulence of different *C. glabrata* strains, the infection model organism *Caenorhabditis elegans* was used, with *Escherichia coli* strain OP50 as a quality control. The protocol followed the instructions of Zhao et al. [55]. Briefly, after washing with M9 buffer three times, *C. elegans* (strain glp-4(bn2) I) at the L4 stage were transferred to brain heart infusion (BHI) medium plates containing yeast or to nematode growth medium (NGM) plates containing OP50 cells. After being incubated at 25 °C for 3 h, the nematodes were washed three times with BHI medium to remove attached microorganisms. About 60 nematodes were then transferred to

each BHI (or NGM) plate, with each group having four identical plates to assure data reliability. The plates were incubated at 25 °C, and nematode survival was recorded every 24 h until all the nematodes were dead. Nematodes were regarded dead if they did not respond to mechanical stimuli, and dead nematodes were instantly removed from the plates throughout the experiment.

Quantitative real-time reverse transcription PCR and transcriptome sequencing analysis

The approach used for qRT-PCR followed the method of Zhao et al. [55]. In short, *C. glabrata* cells in mid-log phase were collected, washed and frozen; then total RNA was isolated using a yeast RNAiso kit (Takara), followed by treatment with gRNA Eraser (Takara) to remove residual genomic DNA. Next, the PrimeScript RT Reagent Kit (Takara) was used to reverse transcribe the purified RNA into cDNA. The mRNA levels of the genes of interest were detected using quantitative real-time PCR (qPCR) with the 7300 Real-Time PCR System (Applied Biosystems, Beijing, China) and TB Green Premix EX Taq (Tli RNaseH Plus, ROX plus) (Takara) according to the manufacturer's instructions. Primers used for qPCR are listed in Table 2 and *ACT1* (encoding actin) served as an endogenous control. Relative changes in gene expression were calculated using the $2^{-\Delta\Delta CT}$ method [57].

For transcriptome sequencing, the protocol was as follows. First, total RNA was extracted from mid-log phase yeast using the TRIzol Reagent (Invitrogen, Waltham, MA, USA) following the manufacturer's instructions, with removal of genomic DNA using DNase I (Takara). After confirming the quality of RNA, a RNA-seq transcriptome library was established following the instructions of the TruSeq RNA sample preparation kit (Illumina, San Diego, CA, USA). Briefly, mRNA was isolated and fragmented. Then, double-stranded cDNA was synthesized using a SuperScript ds-cDNA synthesis kit (Invitrogen). The synthesized cDNA was size selected and PCR amplified for 15 cycles. After being quantified using a TBS380 fluorometer (Turner Biosystems, Sunnyvale, CA, USA), the paired-end RNA-seq sequencing library was sequenced using an Illumina HiSeq xten/NovaSeq 6000 sequencer. After trimming and quality control using SeqPrep (<https://github.com/jstjohn/SeqPrep>) and Sickle (<https://github.com/najoshi/sickle>), clean reads were separately aligned to the reference genome with orientation mode using HISAT2 software [58]. The mapped reads of each sample were assembled by StringTie [59]. To identify DEGs between two different samples, the expression level of each transcript was calculated according to the transcripts per million reads (TPM) method. RSEM [60] was used to quantify gene abundances. Essentially, differential expression analysis

was performed using DESeq2 [61], and genes with $|\log_2$ fold change (FC)| > 1 and Q value ≤ 0.05 were considered to be significantly differentially expressed. In addition, functional-enrichment analysis using Gene Ontology (GO) was performed to identify which DEGs were significantly enriched in GO terms and metabolic pathways, at a Bonferroni-corrected P -value ≤ 0.05 compared with the whole-transcriptome background. GO functional enrichment analysis were carried out by Goatools and KOBAS [62]. The DEG heatmap was generated by the heatmap package of the R software (<https://www.R-project.org/>) based on the results of GO enrichment.

Abbreviations

BHI	Brain heart infusion medium
BSA	Bovine serum albumin
CFW	Calcofluor White
CFU	Colony-forming unit
CLSI	Clinical and Laboratory Standards Institute
ConA	Concanavalin A
CR	Congo Red
CSF	Caspofungin
CWI	Cell wall integrity
DEG	Differential expression gene
ER	Endoplasmic reticulum
FBS	Fetal bovine serum
FLC	Fluconazole
FITC	Fluorescein isothiocyanate
GO	Gene Ontology
ICZ	Itraconazole
MAPK	Mitogen-activated protein kinase
MIC50	50% Minimum inhibitory concentration
NGM	Nematode growth medium
OD	Optical density
PBS	Phosphate-buffered saline
PC	Phosphatidylcholine
PE	Phosphatidylethanolamine
PKC	Protein kinase C
PS	Phosphoserine
qRT-PCR	Quantitative real-time reverse transcription PCR
SDS	Sodium dodecyl sulfonate
TGN	Trans-Golgi network
TPM	Transcripts per million reads
VCZ	Voriconazole
WGA	Wheat germ agglutinin
WT	Wild-type
YPD	Yeast extract peptone dextrose medium

Acknowledgements

Not applicable.

Authors' contributions

Conceptualization: Ke-Zhi Chen and Ming-Jie Xiang; Methodology: Ke-Zhi Chen, Lu-Ling Wang and Jin-Yan Liu; Formal analysis and investigation: Ke-Zhi Chen, Lu-Ling Wang, Si-Jia Huang and Jun-Tao Zhao; Writing—original draft preparation: Ke-Zhi Chen; Writing—review and editing: Lu-Ling Wang and Jin-Yan Liu; Funding acquisition: Ming-Jie Xiang; Resources: Ming-Jie Xiang; Supervision: Ming-Jie Xiang and Jin-Yan Liu. The author(s) read and approved the final manuscript.

Funding

This work was supported by the National Natural Science Foundation of China [#81871706], Shanghai Municipal Health Commission [#202240205], [#201840227] and [#201740069], Natural Science Foundation of Shanghai [#22ZR1439800] and [#15ZR1426900], the Program of Shanghai Key Specialty [#ZK2012A21], and Excellent Youth of HuangPu District of Shanghai [#RCPY1407].

Availability of data and materials

The RNA sequencing data discussed in this study have been deposited in NCBI's Gene Expression Omnibus and are accessible through GEO Series accession number GSE217218 (<https://www.ncbi.nlm.nih.gov/geo/query/acc.cgi?acc=GSE217218>). For reviewer access, please use the following secure token: stwzouukxjgplgl.

Declarations**Ethics approval and consent to participate**

Not applicable.

Consent for publication

Not applicable.

Competing interests

The authors declare that there are no competing interests.

Received: 16 November 2022 Accepted: 2 March 2023

Published online: 13 April 2023

References

- Staniszewska M. Virulence Factors in *Candida* species. *Curr Protein Pept Sci.* 2020;21(3):313–23.
- Kumar K, Askari F, Sahu MS, Kaur R. *Candida glabrata*: A Lot More Than Meets the Eye. *Microorganisms.* 2019;7(2):39.
- Silva S, Negri M, Henriques M, Oliveira R, Williams DW, Azeredo J. *Candida glabrata*, *Candida parapsilosis* and *Candida tropicalis*: biology, epidemiology, pathogenicity and antifungal resistance. *FEMS Microbiol Rev.* 2012;36(2):288–305.
- Pappas PG, Lionakis MS, Arendrup MC, Ostrosky-Zeichner L, Kullberg BJ. Invasive candidiasis. *Nat Rev Dis Primers.* 2018;4:18026.
- Andes DR, Safdar N, Baddley JW, Alexander B, Brumble L, Freifeld A, et al. The epidemiology and outcomes of invasive *Candida* infections among organ transplant recipients in the United States: results of the Transplant-Associated Infection Surveillance Network (TRANSNET). *Transpl Infect Dis.* 2016;18(6):921–31.
- Guinea J. Global trends in the distribution of *Candida* species causing candidemia. *Clin Microbiol Infect.* 2014;20(Suppl 6):5–10.
- Xiao M, Chen SC, Kong F, Xu XL, Yan L, Kong HS, et al. Distribution and Antifungal Susceptibility of *Candida* Species Causing Candidemia in China: An Update From the CHIF-NET Study. *J Infect Dis.* 2020;221(Suppl 2):S139–47.
- Fuller J, Dingle TC, Bull A, Shokoples S, Laverdière M, Baxter MR, et al. Species distribution and antifungal susceptibility of invasive *Candida* isolates from Canadian hospitals: results of the CANWARD 2011–16 study. *J Antimicrob Chemother.* 2019;74(Suppl 4):iv48–54.
- Abi-Said D, Anaissie E, Uzun O, Raad I, Pinzcowski H, Vartivarian S. The epidemiology of hematogenous candidiasis caused by different *Candida* species. *Clin Infect Dis.* 1997;24(6):1122–8.
- Krcmery V, Barnes AJ. Non-albicans *Candida* spp. causing fungaemia: pathogenicity and antifungal resistance. *J Hosp Infect.* 2002;50(4):243–60.
- Perlin DS, Rautemaa-Richardson R, Alastruey-Izquierdo A. The global problem of antifungal resistance: prevalence, mechanisms, and management. *Lancet Infect Dis.* 2017;17(12):e383–92.
- Coste AT, Kritikos A, Li J, Khanna N, Goldenberger D, Garzoni C, et al. Emerging echinocandin-resistant *Candida albicans* and *glabrata* in Switzerland. *Infection.* 2020;48(5):761–6.
- Hassan Y, Chew SY, Than LTL. *Candida glabrata*: Pathogenicity and Resistance Mechanisms for Adaptation and Survival. *J Fungi (Basel).* 2021;7(8):667.
- van der Mark VA, Elferink RP, Paulusma CC. P4 ATPases: flippases in health and disease. *Int J Mol Sci.* 2013;14(4):7897–922.
- Timcenko M, Lyons JA, Janulienė D, Ulstrup JJ, Dieudonné T, Montigny C, et al. Structure and autoregulation of a P4-ATPase lipid flippase. *Nature.* 2019;571(7765):366–70.
- Hiraizumi M, Yamashita K, Nishizawa T, Nureki O. Cryo-EM structures capture the transport cycle of the P4-ATPase flippase. *Science.* 2019;365(6458):1149–55.
- He Y, Xu J, Wu X, Li L. Structures of a P4-ATPase lipid flippase in lipid bilayers. *Protein Cell.* 2020;11(6):458–63.
- Kobayashi T, Menon AK. Transbilayer lipid asymmetry. *Curr Biol.* 2018;28(8):R386–91.
- Zhou X, Sebastian TT, Graham TR. Auto-inhibition of Drs2p, a yeast phospholipid flippase, by its carboxyl-terminal tail. *J Biol Chem.* 2013;288(44):31807–15.
- van Meer G, Voelker DR, Feigenson GW. Membrane lipids: where they are and how they behave. *Nat Rev Mol Cell Biol.* 2008;9(2):112–24.
- Rizzo J, Stanchev LD, da Silva VKA, Nimrichter L, Pomorski TG, Rodrigues ML. Role of lipid transporters in fungal physiology and pathogenicity. *Comput Struct Biotechnol J.* 2019;17:1278–89.
- Muthusamy BP, Natarajan P, Zhou X, Graham TR. Linking phospholipid flippases to vesicle-mediated protein transport. *Biochim Biophys Acta.* 2009;1791(7):612–9.
- Xu D, Zhang X, Zhang B, Zeng X, Mao H, Xu H, et al. The lipid flippase subunit Cdc50 is required for antifungal drug resistance, endocytosis, hyphal development and virulence in *Candida albicans*. *FEMS Yeast Res.* 2019;19(3):foz033.
- Hua Z, Fatheddin P, Graham TR. An essential subfamily of Drs2p-related P-type ATPases is required for protein trafficking between Golgi complex and endosomal/vacuolar system. *Mol Biol Cell.* 2002;13(9):3162–77.
- Takar M, Wu Y, Graham TR. The Essential Neo1 Protein from Budding Yeast Plays a Role in Establishing Aminophospholipid Asymmetry of the Plasma Membrane. *J Biol Chem.* 2016;291(30):15727–39.
- Saito K, Fujimura-Kamada K, Furuta N, Kato U, Umeda M, Tanaka K. Cdc50p, a protein required for polarized growth, associates with the Drs2p P-type ATPase implicated in phospholipid translocation in *Saccharomyces cerevisiae*. *Mol Biol Cell.* 2004;15(7):3418–32.
- Misu K, Fujimura-Kamada K, Ueda T, Nakano A, Katoh H, Tanaka K. Cdc50p, a conserved endosomal membrane protein, controls polarized growth in *Saccharomyces cerevisiae*. *Mol Biol Cell.* 2003;14(2):730–47.
- Huang W, Liao G, Baker GM, Wang Y, Lau R, Paderu P, et al. Lipid Flippase Subunit Cdc50 Mediates Drug Resistance and Virulence in *Cryptococcus neoformans*. *mbio.* 2016;7(3):e00478–16.
- Hu G, Caza M, Bakkeren E, Kretschmer M, Bairwa G, Reiner E, et al. A P4-ATPase subunit of the Cdc50 family plays a role in iron acquisition and virulence in *Cryptococcus neoformans*. *Cell Microbiol.* 2017;19(6). <https://doi.org/10.1111/cmi.12718>.
- Cao C, Wang Y, Husain S, Soteropoulos P, Xue C. A Mechanosensitive channel governs lipid flippase-mediated echinocandin resistance in *Cryptococcus neoformans*. *mBio.* 2019;10(6):e01952–19.
- Mishra M, Huang J, Balasubramanian MK. The yeast actin cytoskeleton. *FEMS Microbiol Rev.* 2014;38(2):213–27.
- Howell AS, Lew DJ. Morphogenesis and the cell cycle. *Genetics.* 2012;190(1):51–77.
- Ksiezopolska E, Schikora-Tamarit M, Beyer R, Nunez-Rodriguez JC, Schüller C, Gabaldón T. Narrow mutational signatures drive acquisition of multidrug resistance in the fungal pathogen *Candida glabrata*. *Curr Biol.* 2021;31(23):5314–26.e10.
- Perlin DS. Echinocandin resistance, susceptibility testing and prophylaxis: implications for patient management. *Drugs.* 2014;74(14):1573–85.
- Dichtl K, Samantaray S, Wagener J. Cell wall integrity signalling in human pathogenic fungi. *Cell Microbiol.* 2016;18(9):1228–38.
- García-Rubio R, de Oliveira HC, Rivera J, Trevijano-Contador N. The Fungal Cell Wall: *Candida*, *Cryptococcus*, and *Aspergillus* Species. *Front Microbiol.* 2019;10:2993.
- Levin DE. Regulation of cell wall biogenesis in *Saccharomyces cerevisiae*: the cell wall integrity signaling pathway. *Genetics.* 2011;189(4):1145–75.
- Walker LA, Gow NA, Munro CA. Elevated chitin content reduces the susceptibility of *Candida* species to caspofungin. *Antimicrob Agents Chemother.* 2013;57(1):146–54.
- Walker LA, Munro CA. Caspofungin Induced Cell Wall Changes of *Candida* Species Influences Macrophage Interactions. *Front Cell Infect Microbiol.* 2020;10:164.
- Chen T, Jackson JW, Tams RN, Davis SE, Sparer TE, Reynolds TB. Exposure of *Candida albicans* β (1,3)-glucan is promoted by activation of the Cek1 pathway. *PLoS Genet.* 2019;15(1): e1007892.

41. Jacobsen ID, Brunke S, Seider K, Schwarzmüller T, Firon A, d'Enfert C, et al. *Candida glabrata* persistence in mice does not depend on host immunosuppression and is unaffected by fungal amino acid auxotrophy. *Infect Immun*. 2010;78(3):1066–77.
42. Seider K, Brunke S, Schild L, Jablonowski N, Wilson D, Majer O, et al. The facultative intracellular pathogen *Candida glabrata* subverts macrophage cytokine production and phagolysosome maturation. *J Immunol*. 2011;187(6):3072–86.
43. Rasheed M, Battu A, Kaur R. Aspartyl proteases in *Candida glabrata* are required for suppression of the host innate immune response. *J Biol Chem*. 2018;293(17):6410–33.
44. Ahamefule CS, Ezeuduji BC, Ogbonna JC, Moneke AN, Ike AC, Jin C, et al. *Caenorhabditis elegans* as an Infection Model for Pathogenic Mold and Dimorphic Fungi: Applications and Challenges. *Front Cell Infect Microbiol*. 2021;11: 751947.
45. Cota JM, Grabinski JL, Talbert RL, Burgess DS, Rogers PD, Edlind TD, et al. Increases in SLT2 expression and chitin content are associated with incomplete killing of *Candida glabrata* by caspofungin. *Antimicrob Agents Chemother*. 2008;52(3):1144–6.
46. Miyazaki T, Inamine T, Yamauchi S, Nagayoshi Y, Saijo T, Izumikawa K, et al. Role of the Slt2 mitogen-activated protein kinase pathway in cell wall integrity and virulence in *Candida glabrata*. *FEMS Yeast Res*. 2010;10(3):343–52.
47. Hankins HM, Sere YY, Diab NS, Menon AK, Graham TR. Phosphatidylserine translocation at the yeast trans-Golgi network regulates protein sorting into exocytic vesicles. *Mol Biol Cell*. 2015;26(25):4674–85.
48. Adams AE, Johnson DI, Longnecker RM, Sloat BF, Pringle JR. CDC42 and CDC43, two additional genes involved in budding and the establishment of cell polarity in the yeast *Saccharomyces cerevisiae*. *J Cell Biol*. 1990;111(1):131–42.
49. Miller KE, Kang PJ, Park HO. Regulation of Cdc42 for polarized growth in budding yeast. *Microb Cell*. 2020;7(7):175–89.
50. Das A, Slaughter BD, Unruh JR, Bradford WD, Alexander R, Rubinstein B, et al. Flippase-mediated phospholipid asymmetry promotes fast Cdc42 recycling in dynamic maintenance of cell polarity. *Nat Cell Biol*. 2012;14(3):304–10.
51. Kishimoto T, Yamamoto T, Tanaka K. Defects in structural integrity of ergosterol and the Cdc50p-Drs2p putative phospholipid translocase cause accumulation of endocytic membranes, onto which actin patches are assembled in yeast. *Mol Biol Cell*. 2005;16(12):5592–609.
52. Rueda C, Cuenca-Estrella M, Zaragoza O. Paradoxical growth of *Candida albicans* in the presence of caspofungin is associated with multiple cell wall rearrangements and decreased virulence. *Antimicrob Agents Chemother*. 2014;58(2):1071–83.
53. Yu SJ, Chang YL, Chen YL. Calcineurin signaling: lessons from *Candida* species. *FEMS Yeast Res*. 2015;15(4):fov016.
54. Tancer RJ, Wang Y, Pawar S, Xue C, Wiedman GR. Development of Antifungal Peptides against *Cryptococcus neoformans*; Leveraging Knowledge about the *cdc50Δ* Mutant Susceptibility for Lead Compound Development. *Microbiol Spectr*. 2022;10(2): e0043922.
55. Zhao JT, Chen KZ, Liu JY, Li WH, Wang YZ, Wang LL, et al. FLO8 deletion leads to decreased adhesion and virulence with downregulated expression of EPA1, EPA6, and EPA7 in *Candida glabrata*. *Braz J Microbiol*. 2022;53(2):727–38.
56. Lee HS, Kim Y. Antifungal Activity of *Salvia miltiorrhiza* Against *Candida albicans* Is Associated with the Alteration of Membrane Permeability and (1,3)- β -D-Glucan Synthase Activity. *J Microbiol Biotechnol*. 2016;26(3):610–7.
57. Livak KJ, Schmittgen TD. Analysis of relative gene expression data using real-time quantitative PCR and the 2⁻($\Delta\Delta$ C_T) Method. *Methods*. 2001;25(4):402–8.
58. Kim D, Langmead B, Salzberg SL. HISAT: a fast spliced aligner with low memory requirements. *Nat Methods*. 2015;12(4):357–60.
59. Pertea M, Pertea GM, Antonescu CM, Chang TC, Mendell JT, Salzberg SL. StringTie enables improved reconstruction of a transcriptome from RNA-seq reads. *Nat Biotechnol*. 2015;33(3):290–5.
60. Li B, Dewey CN. RSEM: accurate transcript quantification from RNA-Seq data with or without a reference genome. *BMC Bioinformatics*. 2011;12:323.
61. Love MI, Huber W, Anders S. Moderated estimation of fold change and dispersion for RNA-seq data with DESeq2. *Genome Biol*. 2014;15(12):550.
62. Xie C, Mao X, Huang J, Ding Y, Wu J, Dong S, et al. KOBAS 2.0: a web server for annotation and identification of enriched pathways and diseases. *Nucleic Acids Res*. 2011;39(Web Server issue):W316–22.

Publisher's Note

Springer Nature remains neutral with regard to jurisdictional claims in published maps and institutional affiliations.

Ready to submit your research? Choose BMC and benefit from:

- fast, convenient online submission
- thorough peer review by experienced researchers in your field
- rapid publication on acceptance
- support for research data, including large and complex data types
- gold Open Access which fosters wider collaboration and increased citations
- maximum visibility for your research: over 100M website views per year

At BMC, research is always in progress.

Learn more biomedcentral.com/submissions

